AFRL-SR-AR-TR-02-

REPORT DOCUMENTATION PAGE

0285

Public reporting burden for this collection of information is estimated to average 1 hour per response, including the time for review ng maintaining the data needed, and completing and reviewing this collection of information. Send comments regarding this burden e suggestions for reducing this burden to Department of Defense, Washington Headquarters Services, Directorate for Information Operations and Reports Suite 1204, Arlington, VA 22202-4302. Respondents should be aware that notwithstanding any other provision of law, no person shall be subject to any penalty for failing to comply with a collection of information if it does not display a currently valid OMB control number. PLEASE DO NOT RETURN YOUR FORM TO THE ABOVE ADDRESS.

1. REPORT DATE (DD-MM-YYYY)	2. REPORT TYPE	3. DATES COVERED (From - To)
25-07-2002	Research	From 01-07-98 to 30-01-02

4. TITLE AND SUBTITLE
Fabrication of and Transport Study on $YBa_2Cu_3O_{7-\delta}/PrBa_2(Cu_{1-x}M_x)_3O_7$ Type Multilayers

5a. CONTRACT NUMBER

5b. GRANT NUMBER
F49620-98-1-0488

5c. PROGRAM ELEMENT NUMBER

6. AUTHOR(S)
Dr. Tar-pin Chen

5d. PROJECT NUMBER
3484/BS

5e. TASK NUMBER

5f. WORK UNIT NUMBER

7. PERFORMING ORGANIZATION NAME(S) AND ADDRESS(ES)
University of North Dakota
Grand Fork, ND 58202-7129

20020909 132

9. SPONSORING / MONITORING AGENCY NAME(S) AND ADDRESS(ES)
AFSOR/NE
110 Duncan Avenue, Room B115
Bolling AFB DC 20332-8050

10. SPONSOR/MONITOR'S ACRONYM(S)
DEPSCoR

11. SPONSOR/MONITOR'S REPORT NUMBER(S)

12. DISTRIBUTION / AVAILABILITY STATEMENT
Some of the research results have been published in journals. More publications are under preparation.

13. SUPPLEMENTARY NOTES
The research results has led to another DoD funding for making SIS Josephson junctions and devices

14. ABSTRACT
Ceramic samples of $PrBa_2(Cu_{1-x}M_x)_3O_7$ (PBCMO) were fabricated by substituting M = Al, Co, Fe, Ga, Ni, and Zn partially for Cu with substituting level x = 0.00, 0.05, 0.10, 0.15, and 0.20. X-ray diffraction shows that the lattice parameter of all PBCMO samples are very close to that of $YBa_2Cu_3O_{7-\delta}$ (YBCO) while transport measurement indicated that the resistivities of all doped samples are order of magnitude higher than $PrBa_2Cu_3O_7$ (PBCO). PBCMOs, therefore, are better insulator for YBCO then PBCO. $PrBa_2(Cu_{0.8}Al_{0.2})_3O_7$ (PBCAO) and $PrBa_2(Cu_{0.8}Ga_{0.2})_3O_7$ (PBCG) were used as buffer layers for YBCO multilayers. Transport studies show that for a give thickness of YBCO layer the superconducting transition temperatures T_c for all multilayers are the same in spite of the thickness of the buffer layers. This indicated that the buffer layers made of the PBCAO and PBCGO can effectively insulates the YBCO in the multilayers even when the thickness of the buffer layer is only 12.5 Å. Increasing YBCO increases T_c. However, T_c reaches a maximum when the YBCO thickness reaches 100 Å indicating the superconducting length is ~ 100 Å. These materials could be ideal buffer layer for SIS Josephson junctions/devices.

15. SUBJECT TERMS

16. SECURITY CLASSIFICATION OF:			17. LIMITATION OF ABSTRACT	18. NUMBER OF PAGES	19a. NAME OF RESPONSIBLE PERSON
a. REPORT	b. ABSTRACT	c. THIS PAGE			19b. TELEPHONE NUMBER (include area code)

Standard Form 298 (Rev. 8-98)
Prescribed by ANSI Std. Z39.18

Approved for Public Release
Distribution Unlimited

Research Report

I. The Focus of the Research Project

It is known that the problem in high transition temperature (T_c) superconducting electronics is the lack of effective I-layer materials for the SIS Josephson junctions. $PrBa_2Cu_3O_7$ (**PBCO**) has been considered to be the best buffer layer for $YBa_2Cu_3O_{7-\delta}$ (**YBCO**) multilayer/superlattice because of its excellent lattice parameters match with YBCO, same fabricating conditions, and its semiconductor/insulator behavior. However, experiments indicated that when a PBCO film is in good contact with a YBCO film, the PBCO film will be induced into a conductor. This makes PBCO inadequate to insulate the YBCO layers in a SIS junction nor to be an effective buffer layer for YBCO/PBCO type multilayer/superlattice.

The main purpose of this research is to find materials that can be served as buffer layer for YBCO so that the coupling between YBCO layers fabricated on each side of the buffer layer can be cut off and each YBCO layer in the superlattice is independent to the others. It is widely believed that superconductivity of YBCO is generated from the CuO_2 planes – a 2-D superconductor. When the YBCO layer in the multilayer/superlattice is made very thin, the YBCO layer may be considered as a two-dimensional (2-D) entity. The superlattice can therefore be used to study the existence of 2-D superconducting transition. The CuO_2 planes in YBCO may couple to each other. The coupling thus makes YBCO a three-dimension superconductor. By increasing the thickness of YBCO layer the superconducting conducting coupling between the CuO_2 planes can be studied.

II. Studies on Bulk Materials

It is well known that when Cu in YBCO is replaced by other metal elements, T_c goes down indicating that metal substitution lowers the electrical conduction of the YBCO. Since PBCO has same crystal structure as YBCO, Cu substituted by metal element may also increase the electrical resistivity in PBCO. This may improve the insulation of PBCO on YBCO. For this reason, metal element M = Al, Co, Fe, Ga, Ni and Zn were used to partially replace Cu in PBCO. In other words, we have fabricated $PrBa_2(Cu_{1-y}M_y)_3O_7$ (**PBMCO**), in which y = 0.00, 0.05, 0.10, 0.15, and 0.20 is the doping level.

A. X-ray and Neutron Diffraction Studies

Figure 1 shows the powder x-ray diffraction spectra of $PrBa_2(Cu_{0.8}M_{0.2})_3O_7$, for M= Al, Fe, and Ni, while Figure 2 (a), (b), and (c) shows those for M= Ga, Zn, and Co. All reflections can be indexed in the orthorhombic *Pmmm* space group. The sample-indexed peaks of YBCO and PBCO are shown in Figure 3. The data show diffraction patterns consistent with those expected for the *Pmmm* space group. The x-ray spectra for most samples show that the samples are of single-phase oxygen deficient perovskite structure. However, when the doping concentration $x \geq 0.15$ a minor impurity phase appears in Ni and Zn-doped samples. The impurity phase was identified as $BaCO_3$. It has also been shown that the orthorhombicity of the M doped-PBCO samples is less than that of the undoped PBCO. Our final refinements on x-ray

and neutron diffraction data for the orthorhombic structure have been carried out in the tetragonal space group *Pmmm*. Attempts to refine in other space groups including the *P4/mmm* give either incomparable or poorer fits to the data. Multiphase analyses for the neutron diffraction data give better fits. The profiles of Rietveld refinements for orthorhombic $PrBa_2(Cu_{0.80}Al_{0.20})_3O_7$ are shown in Figure 4. The essential features of the orthorhombic structure, atomic coordinates, and the number of occupancy for each atom in $PrBa_2(Cu_{0.8}Al_{0.2})_3O_7$ are given in Table 1. The lattice parameters for all samples obtained through Rietveld refinement on the x-ray diffraction data are given in Table 2.

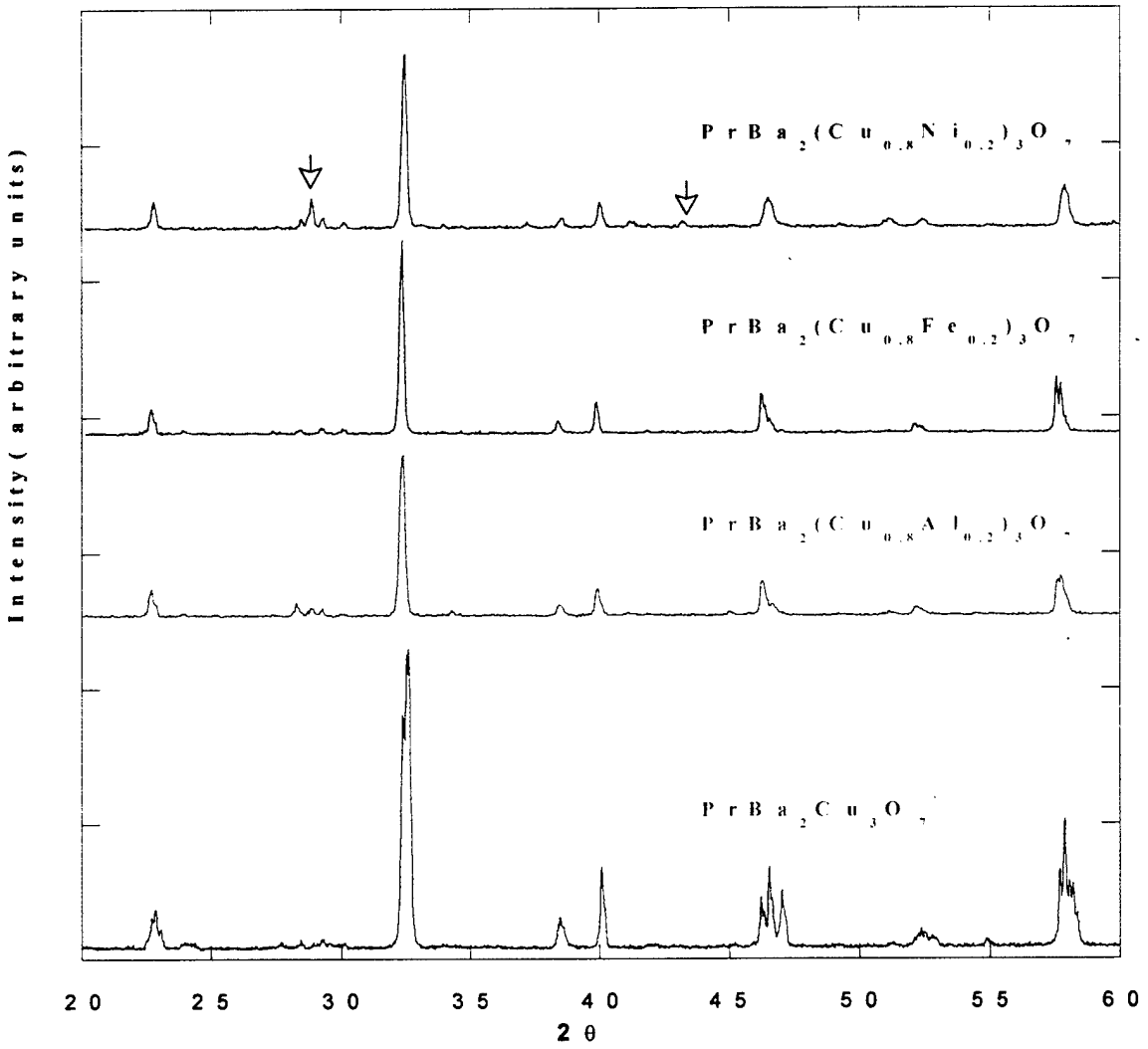

Figure 1 X-ray diffraction spectra of $PrBa_2(Cu_{0.8}M_{0.2})_3O_7$ for M= Al, Fe, and Ni taken at room temperature. The arrows show the impurity phase.

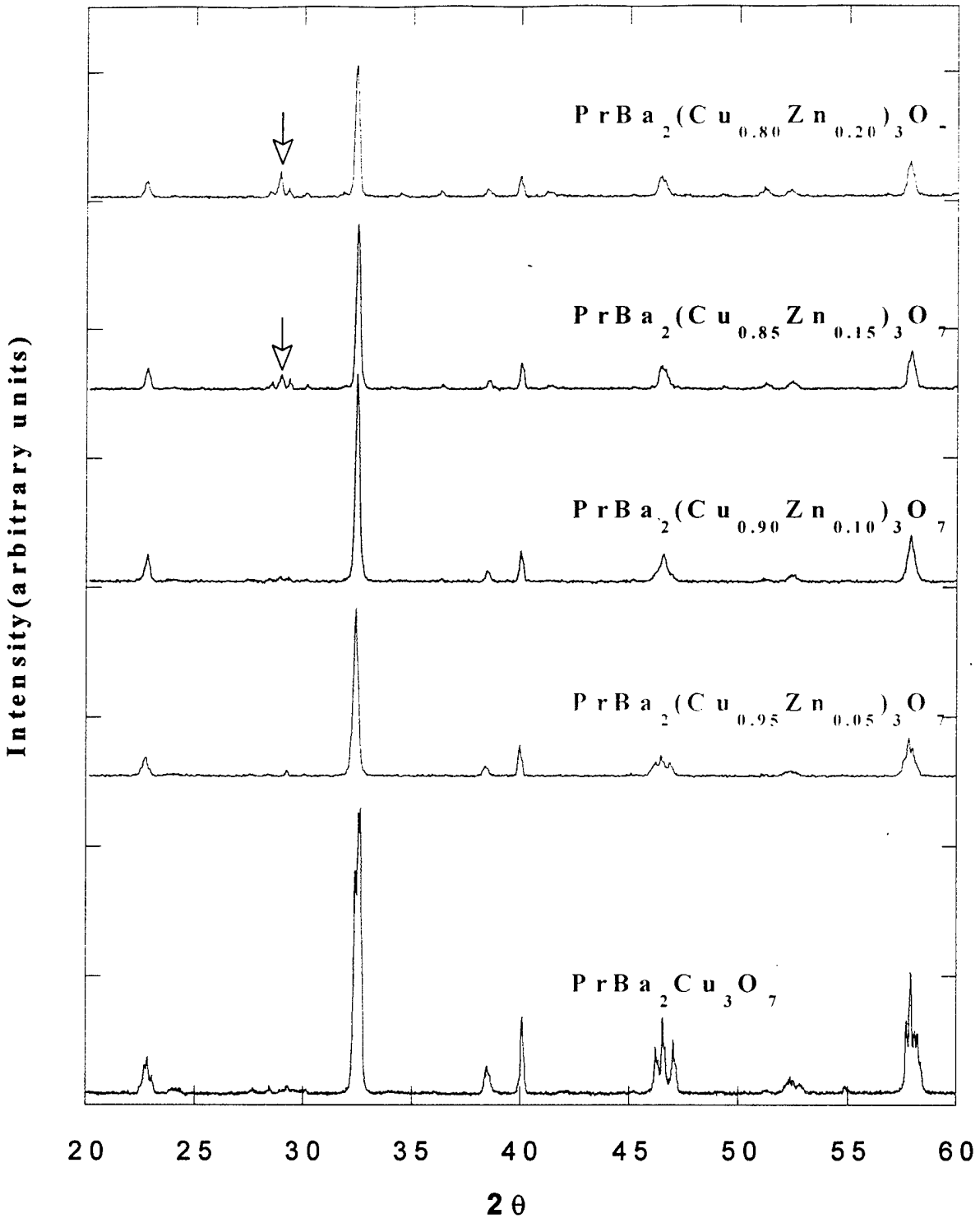

Figure 2 (a) Room temperature x-ray diffraction patterns for $PrBa_2(Cu_{1-x}\ Zn_x)_3O_7$, where x = 0.00, 0.05, 0.10, and 0.20. The arrows indicate the peaks from impurity phase.

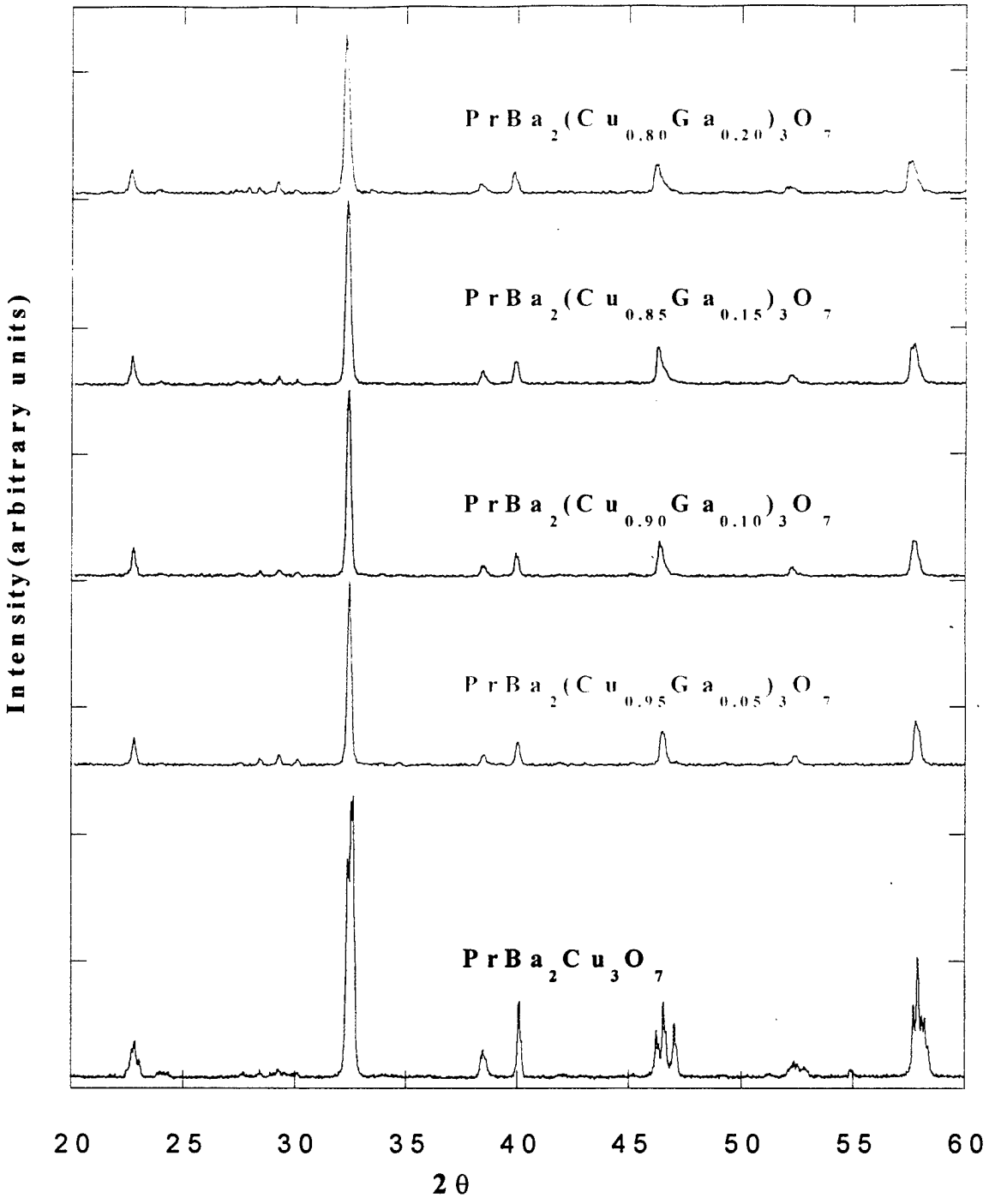

Figure 2 (b) Room temperature x-ray diffraction patterns of $PrBa_2(Cu_{1-x}Ga_x)_3O_7$, where x = 0.00, 0.05, 0.10, and 0.20.

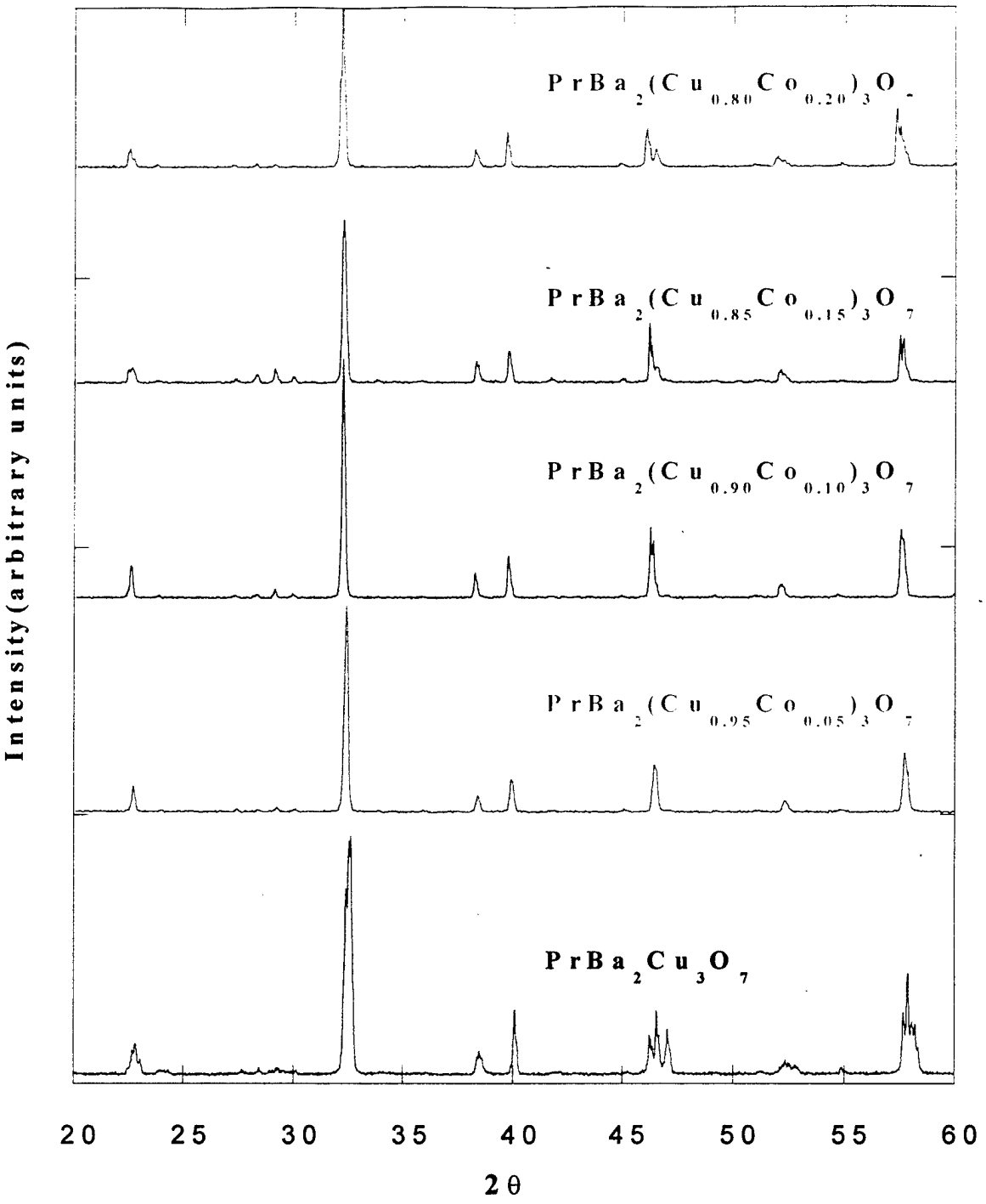

Figure 2 (c) Room temperature x-ray diffraction patterns of $PrBa_2(Cu_{1-x}Co_x)_3O_7$, where x = 0.00, 0.05, 0.10, and 0.20.

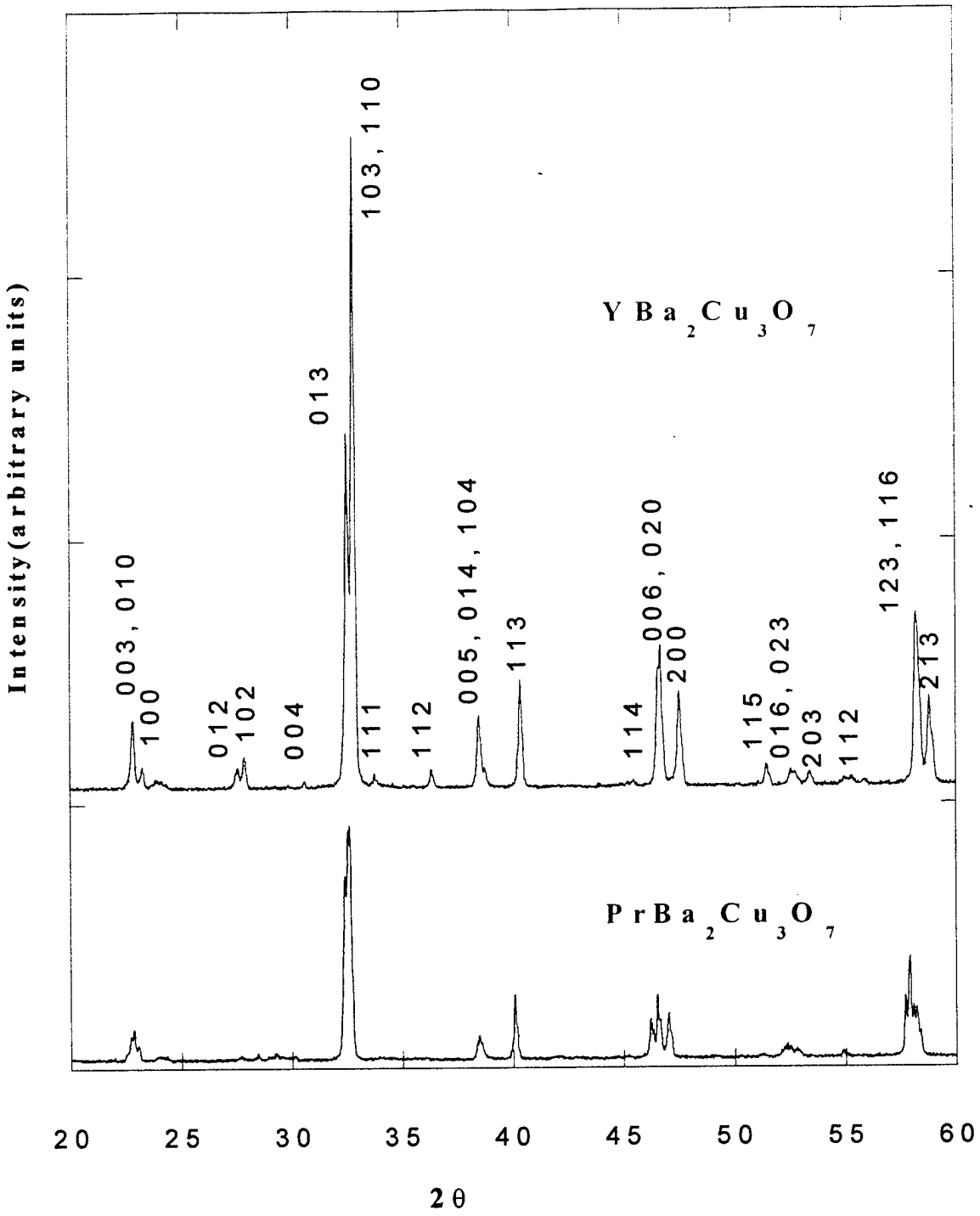

Figure 3 The reflection indices of x-ray diffraction patterns for $YBa_2Cu_3O_7$ and $PrBa_2Cu_3O_7$.

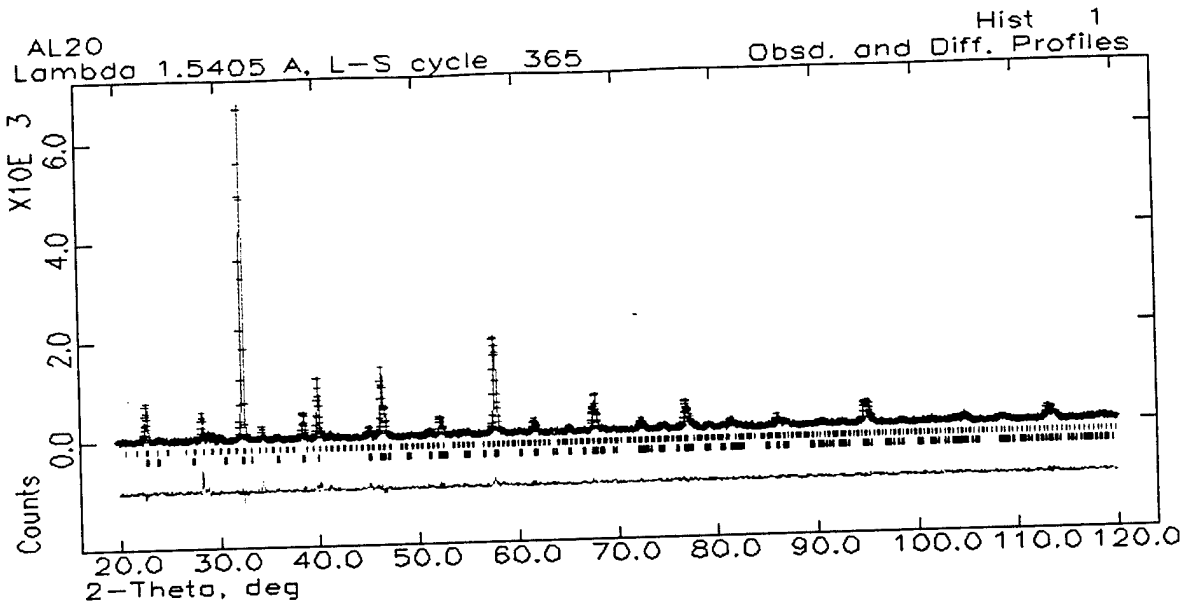

(a)

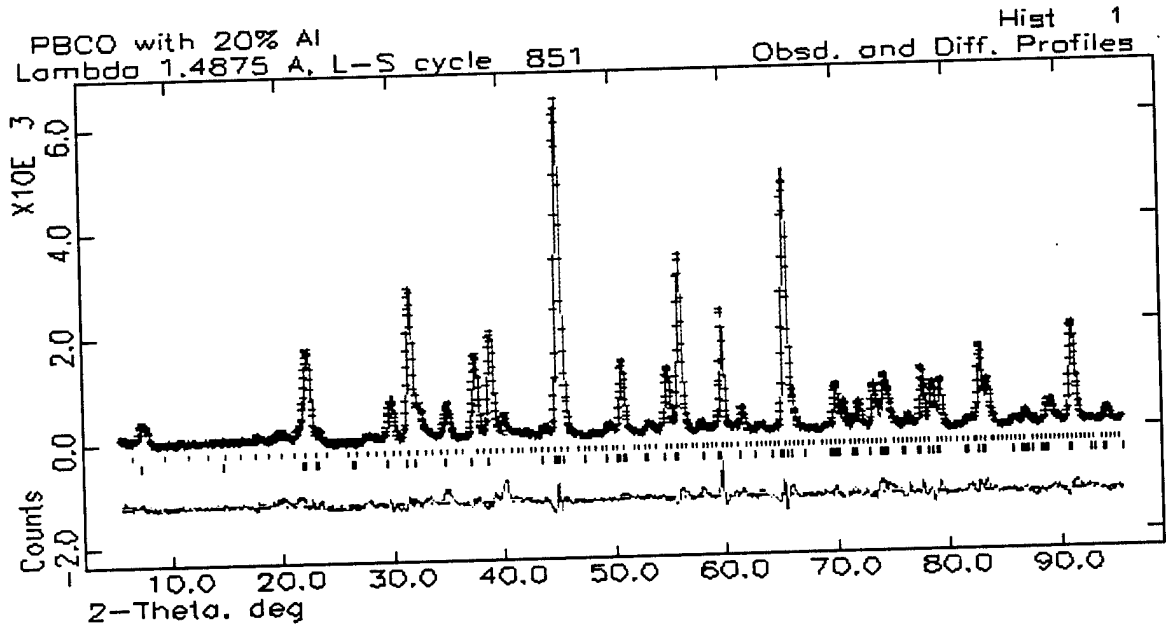

(b)

Figure 4 Rietveld refinement profiles of (a) x-ray and (b) neutron diffraction data for $PrBa_2(Cu_{0.08}Al_{0.02})_3O_7$ at room temperature. Plus marks (+) are the observed data and the continuous lines are the calculated profiles. Tick marks below the curves indicate the positions of the allowed $PrBa_2(Cu_{0.08}Al_{0.02})_3O_7$ reflections (upper tick marks) and the minor $BaCaO_3$ impurity phase reflections (lower tick marks) included in the refinements.

Table 1 Structure parameters for orthorhombic $PrBa_2(Cu_{0.80}Al_{0.20})_3O_7$ determined from a joint refinement of x-ray and neutron diffraction data taken at room temperature.

Space Group *Pmmm*, a = 3.9146(8), b = 3.9090(8), c = 11.6802(11)

Atom	x	y	z	B_{iso}(Å^2)	Occupancy
Pr	0.5	0.5	0.5	0.0084	1
Ba	0.5	0.5	0.179593	0.0127	0.9871
Cu(1)	0	0	0	0.0620	0.8
Cu(2)	0	0	0.349970	0.0036	1
O(1)	0	0.5	0	0.0291	0.5889
O(2)	0.5	0	0.372561	0.0131	1
O(3)	0	0.5	0.372559	0.0172	1
O(4)	0	0	0.157350	0.0375	1
O(5)	0.5	0	0	0.0360	0.05732
Al@Cu(1)	0	0	0	0.0620	0.2

Table 2 The lattice parameters for $YBa_2Cu_3O_7$ and $PrBa_2(Cu_{1-x}M_x)_3O_7$.

Composition	a(Å)	b(Å)	c(Å)	V(Å^3)
$YBa_2Cu_3O_7$[43]	3.8218(7)	3.8913(7)	11.677(2)	173.657(11)
$PrBa_2Cu_3O_{7-\delta}$	3.90608(46)	3.92504(42)	11.63817(129)	178.433(49)
$PrBa_2(Cu_{1-x}Al_x)_3O_{7-\delta}$				
x = 0.05	3.91511(27)	3.91660(27)	11.69780(39)	179.373(10)
x = 0.10	3.91198(60)	3.91476(53)	11.70080(146)	179.187(45)
x = 0.15	3.92081(59)	3.92519(54)	11.67906(150)	179.740(53)
x = 0.20	3.9146(8)	3.9090(8)	11.6802(11)	178.732(22)
$PrBa_2(Cu_{1-x}Fe_x)_3O_{7-\delta}$				
x = 0.05	3.91108(87)	3.91348(93)	11.73872(290)	179.672(43)
x = 0.10	3.91731(95)	3.91903(85)	11.73948(161)	180.225(39)
x = 0.15	3.92383(61)	3.92728(55)	11.72063(144)	180.615(47)
x = 0.20	3.92372(86)	3.92496(85)	11.70641(136)	180.284(45)
$PrBa_2(Cu_{1-x}Ga_x)_3O_{7-\delta}$				
x = 0.05	3.91092(59)	3.91634(51)	11.70261(165)	179.243(53)
x = 0.10	3.91738(48)	3.92439(41)	11.70455(130)	179.938(45)
x = 0.15	3.92052(90)	3.93069(82)	11.69938(246)	180.291(93)
x = 0.20	3.92032(60)	3.93380(55)	11.69724(166)	180.392(64)
$PrBa_2(Cu_{1-x}Ni_x)_3O_{7-\delta}$				
x = 0.05	3.90433(49)	3.91607(43)	11.66708(137)	178.385(51)
x = 0.10	3.90247(57)	3.91207(47)	11.67310(157)	178.210(55)
x = 0.15	3.90374(75)	3.91515(63)	11.67351(206)	178.415(75)
x = 0.20	3.90379(123)	3.91523(101)	11.67141(331)	178.388(122)
$PrBa_2(Cu_{1-x}Zn_x)_3O_{7-\delta}$				
x = 0.05	3.90503(47)	3.92735(43)	11.64535(138)	178.598(51)
x =0.10	3.90509(48)	3.92233(42)	11.67745(143)	178.865(52)
x = 0.15	3.90876(68)	3.92132(59)	11.68568(191)	179.112(71)
x = 0.20	3.91032(89)	3.92262(77)	11.68899(248)	179.294(92)
$PrBa_2(Cu_{1-x}Co_x)_3O_{7-\delta}$				
x = 0.05	3.9143(6)	3.9193(6)	11.7267(19)	179.90(5)
x = 0.10	3.9180(10)	3.9210(11)	11.7294(19)	180.19(7)
x = 0.15	3.9251(12)	3.9307(11)	11.7193(19)	180.81(8)
x = 0.20	3.9348(11)	3.9367(12)	11.7167(18)	181.49(8)

Table 4.2 lists the lattice parameters of all PBCMO samples and $YBa_2Cu_3O_7$ for comparison. The lattice parameters for all PBCMO samples are very close to those of $YBa_2Cu_3O_7$. These results indicate that the structure and the lattice parameters of the PBCMO samples and $YBa_2Cu_3O_7$ are very compatible.

B. Electrical resistivity of the doped samples

Figure 5 shows the plots of electrical resistivity versus temperature for all samples. Below 100 K, the electrical resistivity for all doped samples are orders of magnitude higher than that of the undoped sample which indicates that the doped samples are much better insulators than the undoped PBCO. For this reason and for their excellent lattice match with YBCO, all of the doped samples should be better buffer layers than the undoped PBCO for making YBCO/PBCMO superlattices and SIS junctions.

Among these samples Fe, Ni, and Co have magnetic moments. Al, Zn, and Ga are non magnetic. In general, substituting magnetic elements for Cu in YBCO suppresses the T_c of YBCO because the intrinsic magnetic field of the magnetic element may break the Cooper pairs. Among all of the doped samples, the electrical resistivity of Zn-doped samples is the lowest. Zn-doped YBCO has also been found to reduce the T_c of YBCO significantly. Migration of the magnetic atoms and Zn into the YBCO layers from the PBCMO layers in the superlattice may lower the T_c of the superlattice. Zn, Fe, Co, and Ni-doped PBCO thus may not be ideal buffer layers for making YBCO/PBCMO multilayers. Among all doped samples, Al-doped and Ga-doped samples have the highest and second highest electrical resistivity than any other doped samples. For these reasons, Al and Ga-doped PBCO may be the best candidates to serve as the buffer layers in YBCO multilayers.

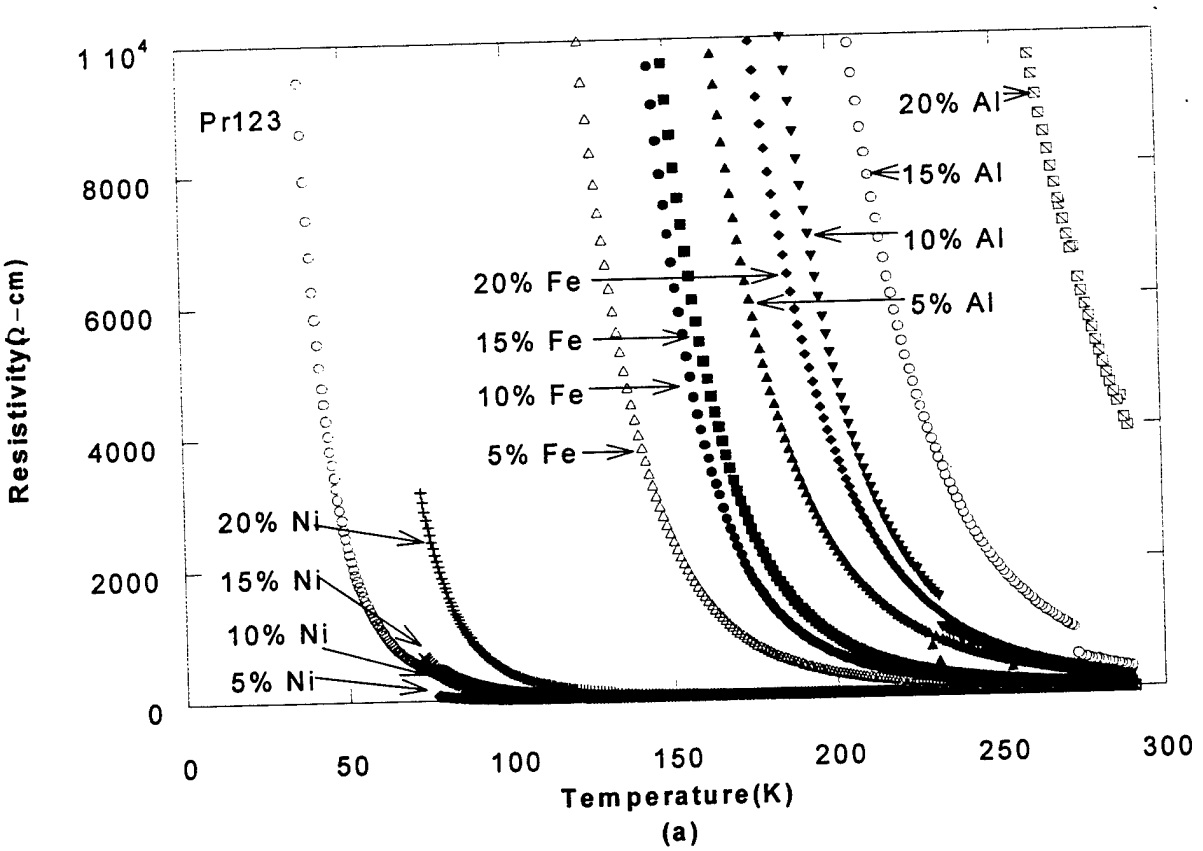

Figure 5(a) Electrical resistivity verses temperature for PBCMO samples of M = Ni, Fe.

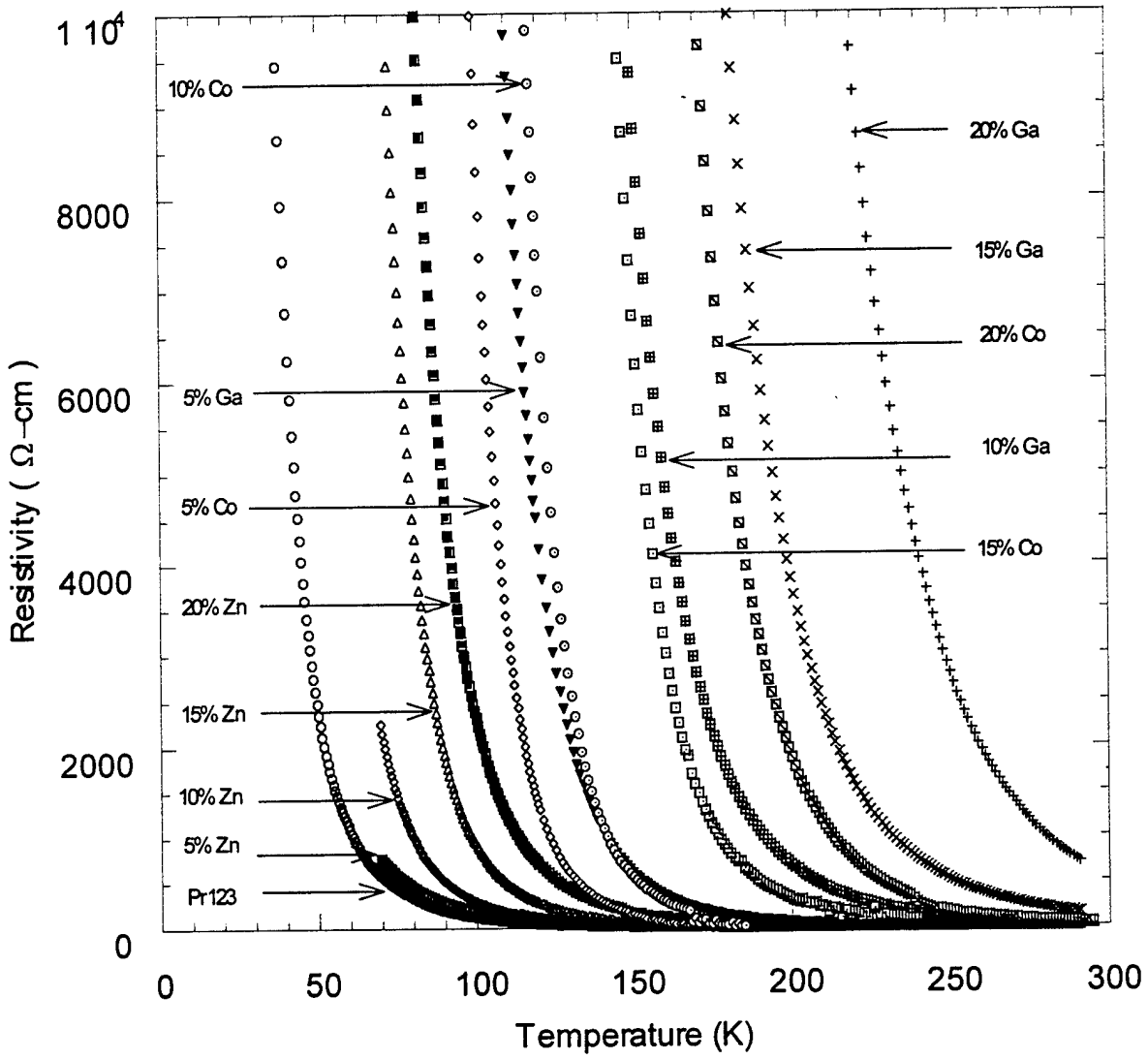

Figure 5(b) Electrical resistivity verses temperature for PBCMO samples of M = Zn, Co, and Ga.

IV Thin Films and Multilayer Studies

A. Quality of $PrBa_2(Cu_{0.80}Al_{0.20})_3O_7$ and $PrBa_2(Cu_{0.80}Ga_{0.20})_3O_7$ films

X-ray diffraction of $PrBa_2(Cu_{0.80}Al_{0.20})_3O_7$ (**PBCAO**) thin films grown by rf sputtering indicates a high degree of orientation with the c-axis perpendicular to the substrate, as shown in Figure 6. Figure 7 (a) and (b), on the other hand, show x-ray diffraction pattern of a 2000Å thick PBCAO and a $PrBa_2(Cu_{0.80}Ga_{0.20})_3O_7$ (**PBCGO**) films grown by pulse laser ablation on $NdGaO_3$ (110) substrate. The figures show the dominant features on x-ray spectra are the (00n) peaks of n= 2, 3, 4, 5, 6, 7. Theses results indicate that the films are highly oriented along the c-axis which is normal to the substrate surface.

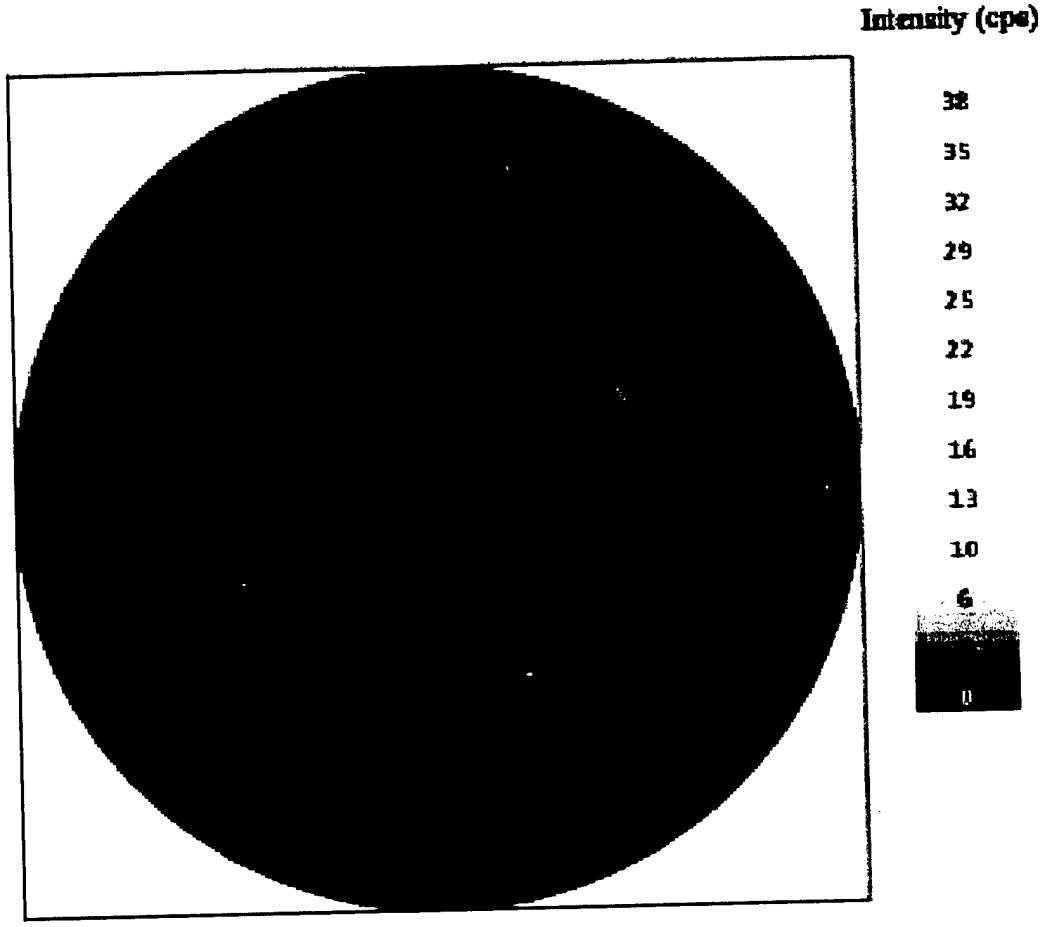

Figure 6 X-ray (001) pole figure plot of the PBCAO film on (001) $LaAlO_3$ shows the four {111} peaks.

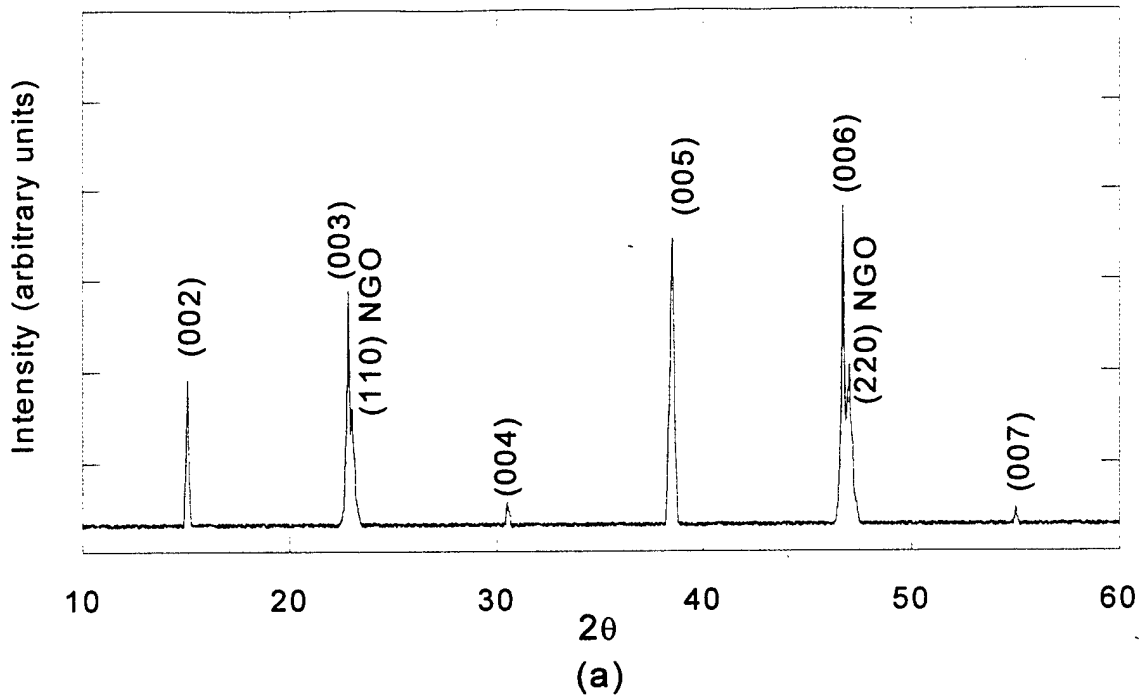

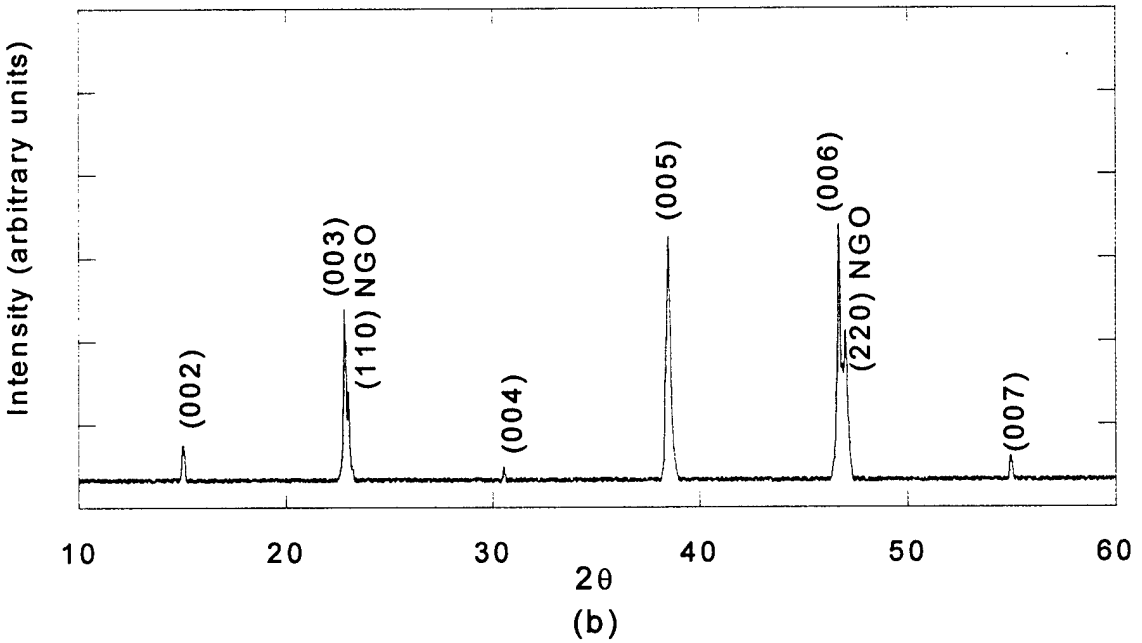

Figure 7 X-ray diffraction spectrum of 2000Å (a) PBCAO and (b) PBCGO films grown by pulsed laser ablation. The peaks indicate that the films are c-axis oriented

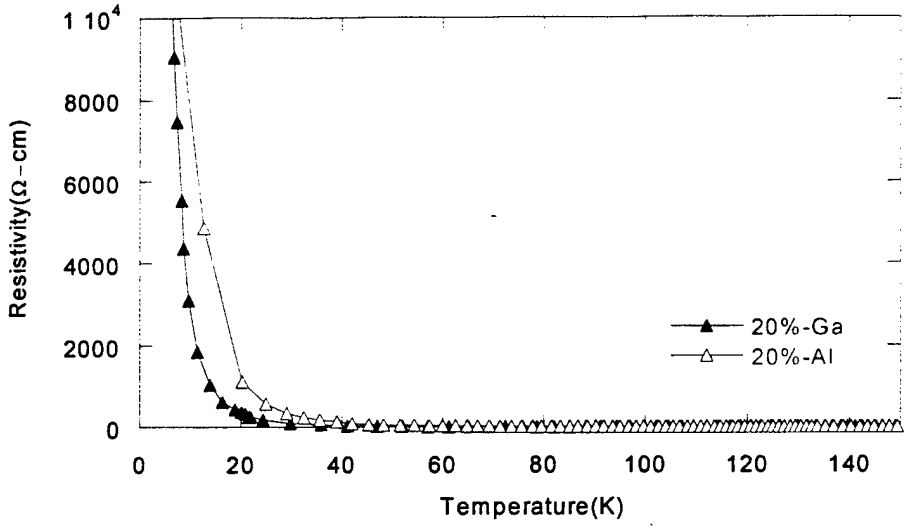

Figure 8 Resistivity plotted against temperature for c-axis orientated PBCAO and PBCGO films grown by pulsed laser ablation.

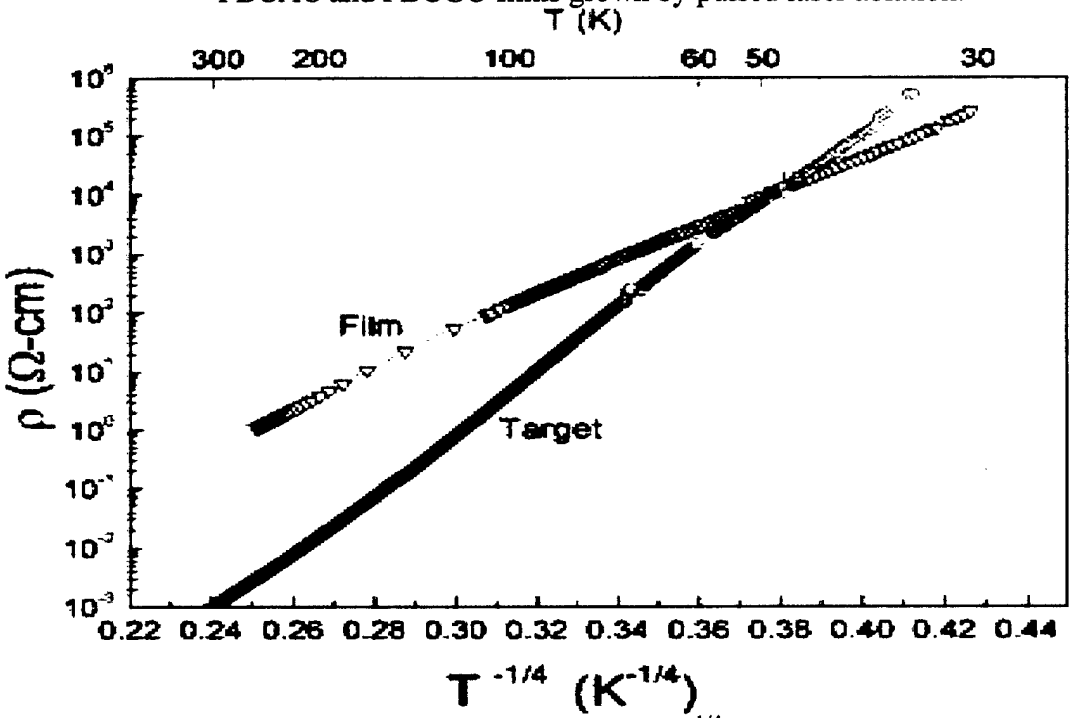

Figure 9 Semilog plot of electrical resistivity (ρ) vs $T^{-1/4}$ for PBCAO target (bulk) and thin film.

Figure 8 shows the plots of the electrical resistivity vs. temperature for c-axis orientated PBCAO and PBCGO films grown by pulsed laser ablation. The plots indicate that the films may serve as a buffer layer for the YBCO/PBCMO multilayers. Materials with localized charge carriers, in principle, follows the Mott's variable range hopping (VRH) mechanism, $\rho = \rho_0 e^{(T_0/T)^p}$. Figure 9 shows the resistivity $\rho(T)$ for the thin film and target of PBCAO (bulk

sample) plotted against $T^{-1/4}$. Both the film and bulk sample follow a reasonable straight line suggests that the transport mechanism of the samples is largely through three-dimensional thermally activated variable range hopping of charge carriers among the localized states. The resistivity of the film is higher than that of the bulk at temperature above 48 K. But the less slanted $\rho(T)$ verse T curve suggests that the charge carriers in the film are less localized than those in the bulk sample.

D. Superconductivity of YBCO/PBCMO superlattices

Figure 10 and Figure 11 plots the temperature dependence of dc resistance for PBCAO (60Å)/YBCO(d)/PBCAO(200Å) trilayers and PBCGO(60Å)/YBCO(d)/PBCGO(25Å)/YBCO(d) /PBCGO (200 Å) 5 layer in which the YBCO thickness d = 1, 2, 3, 4, 6, 8, and 16 unit cells or 12.5 Å, 25Å, 37.5Å, 50Å, 75Å, 100Å, and 200Å. In these measurements, no superconducting transition was observed above 4.2 K for superlattices made of 12.5 Å thick YBCO films in superlattices of 3, 5, 7, and 9 layers. However, $\rho(T)$ verse T curves for YBCO/PBCGO and YBCO/PBCAO superlattices made of 25 Å of YBCO give a 50 K onset transition temperature. (note that we have 25Å YBCO data for both PBCAO and PBCGO superlattice). The onset transition temperature of 3, 5, and 7 layers with the varied thickness of YBCO was summarized in the Figure 12. The transition temperature of the superlattices made of 100 Å and 200 Å thick YBCO in buffer layers PBCAO and PBCGO are the same within experimental uncertainty and are about 90 K. This result indicates that the superconducting coupling length of YBCO is about 100Å.

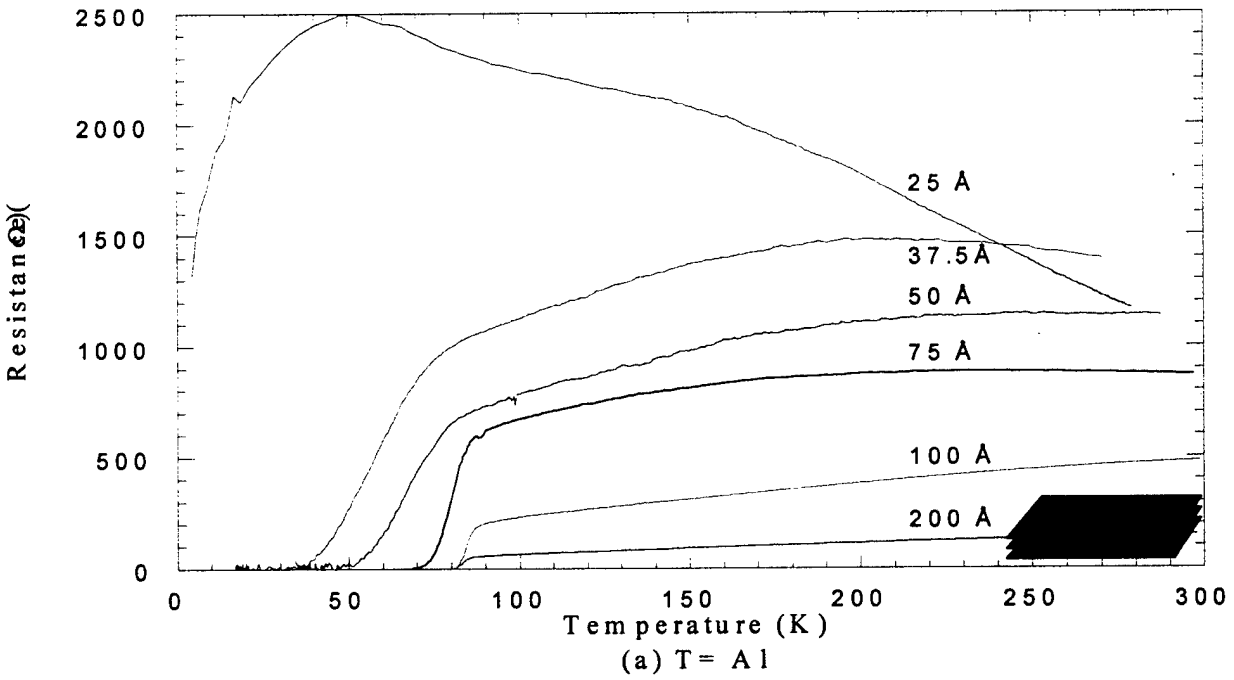

Figure 10 The plots of temperature versus dc resistance for (a) PBCAO (60 Å)/ YBCO(d)/ PBCAO (200 Å), and (b) PBCGO (60 Å)/ YBCO(d)/ PBCGO (200 Å) multilayers of different d.

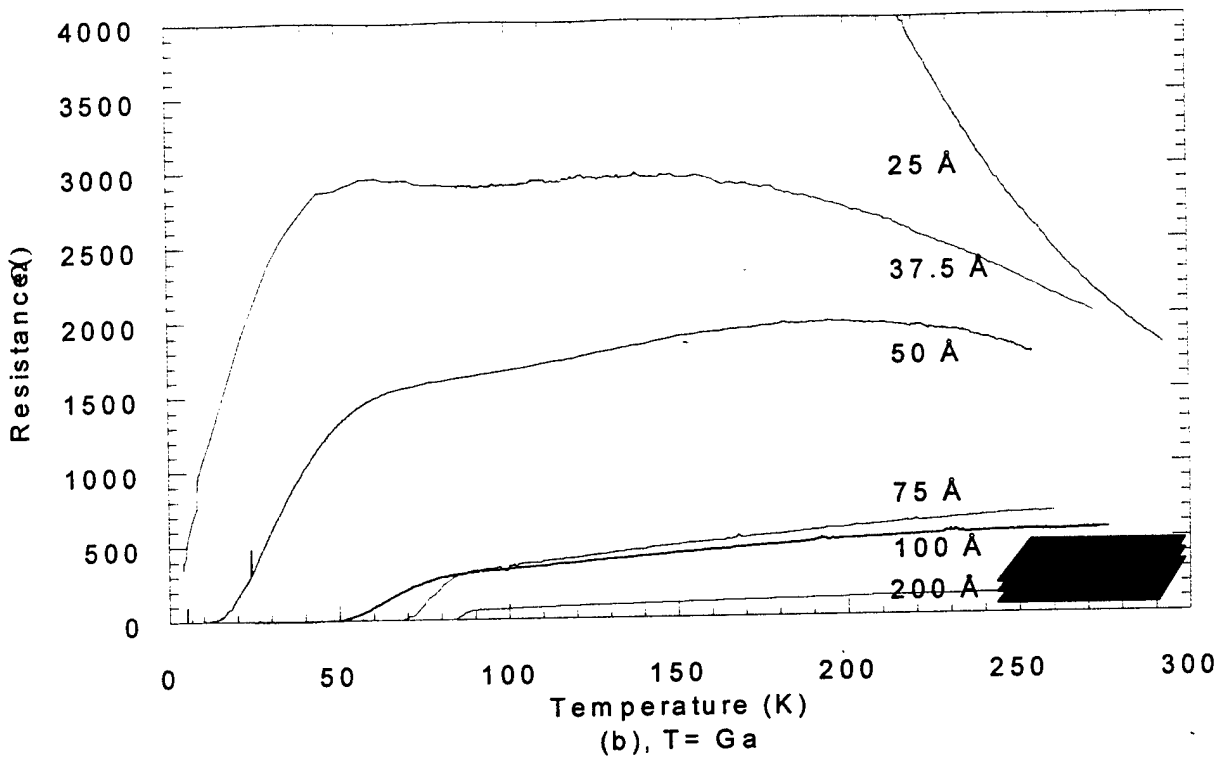

Figure 11 The plots of temperature versus relative resistivity for 5 layers of PBCGO (60 Å)/YBCO (d)/PBCGO (24 Å)/YBCO/PBCGO (200 Å) multilayers with YBCO thickness varied.

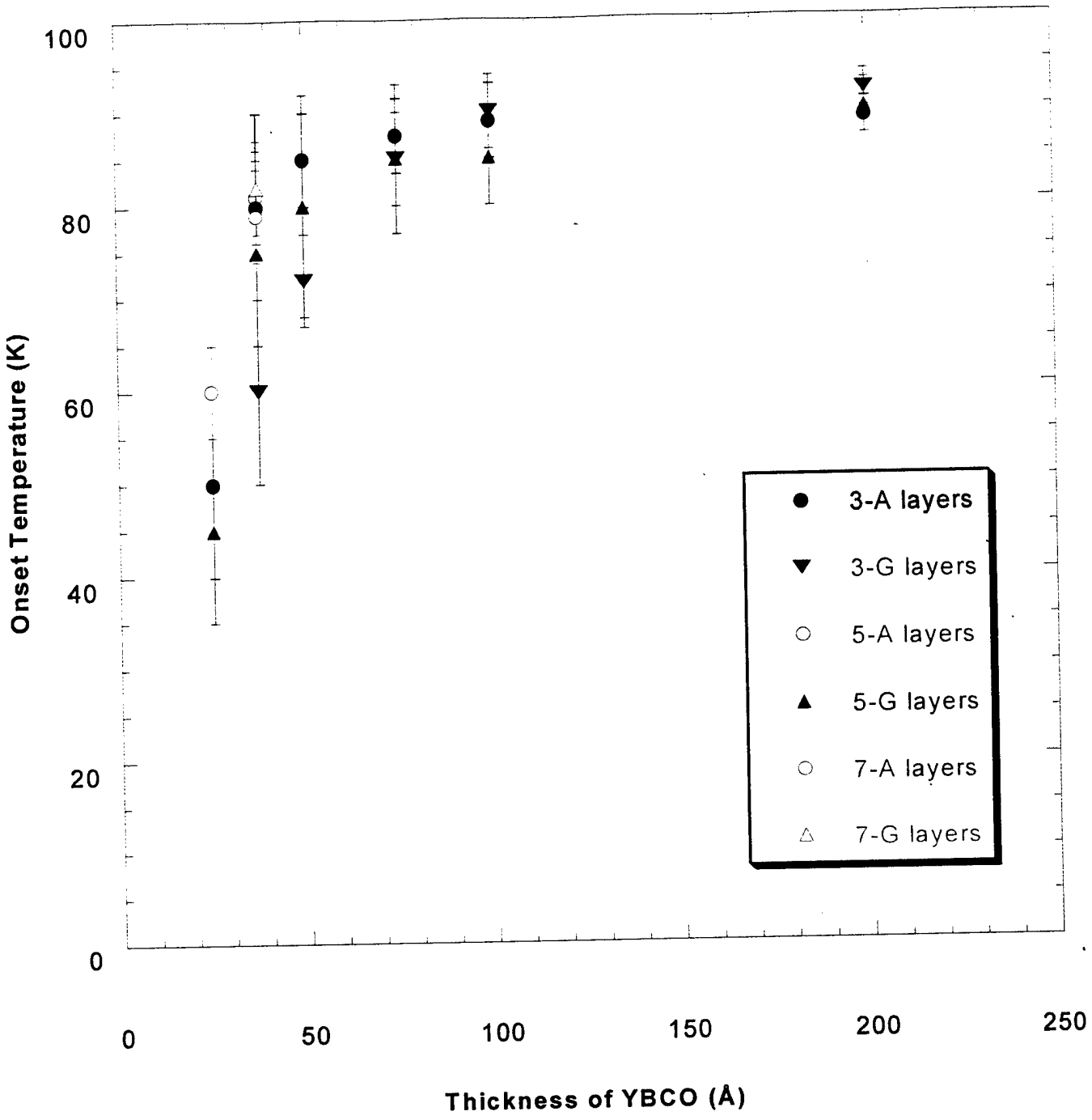

Figure 12. T_c onset versus YBCO thickness for 3, 5, and 7 layers superlattices

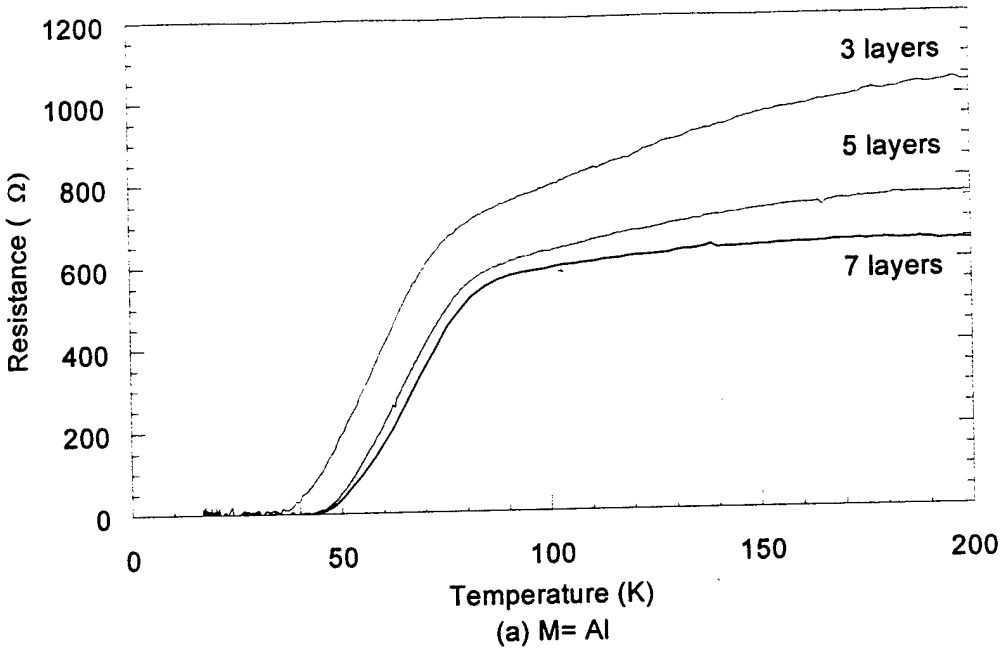

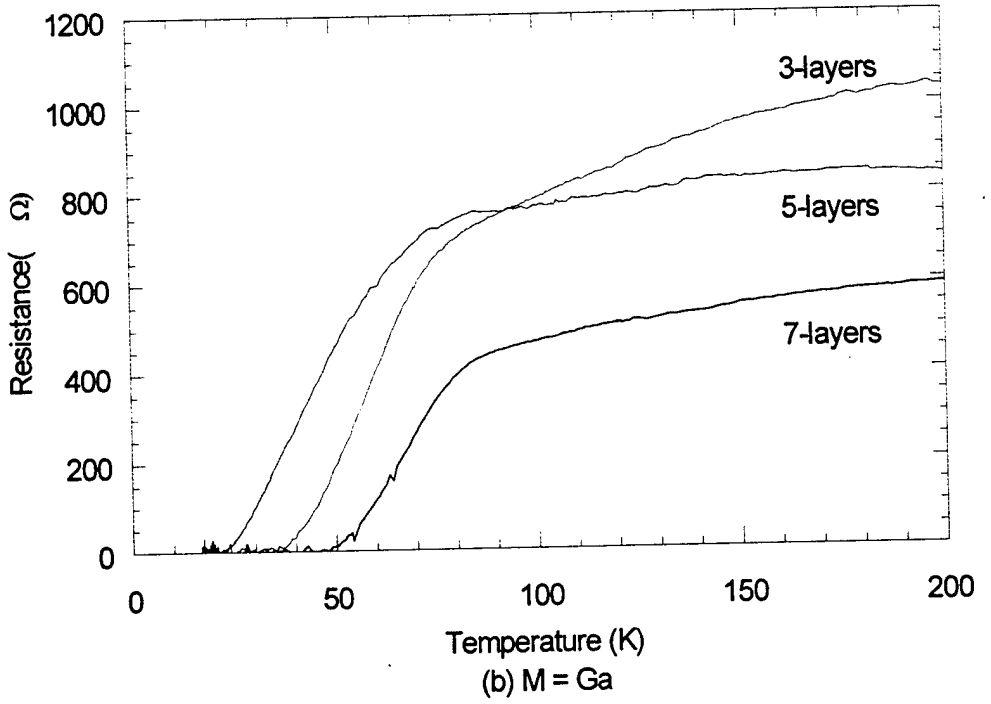

Figure 13. Resistance versus temperature for 3, 5, and 7 layers PBCMO/YBCO superlattices with YBCO thickness fixed at 37.5 Å.

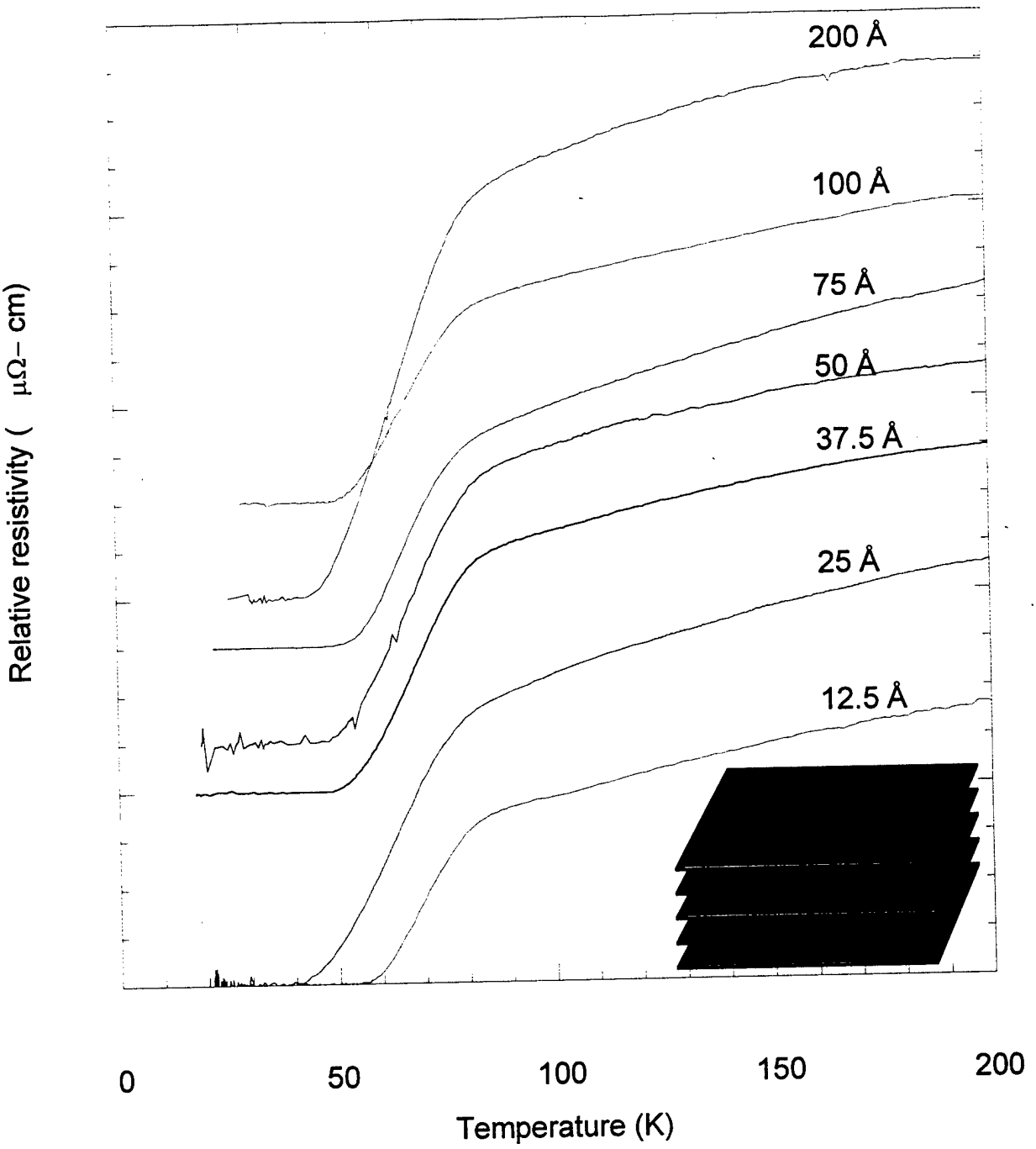

Figure 14 Relative resistivity versus temperature for 5 layers A (60 Å)/YBCO (37.5 Å) /A(varied)/ YBCO (37.5 Å)/ A (200 Å) superlattices with PBCAO thickness varied, where A = PBCAO.

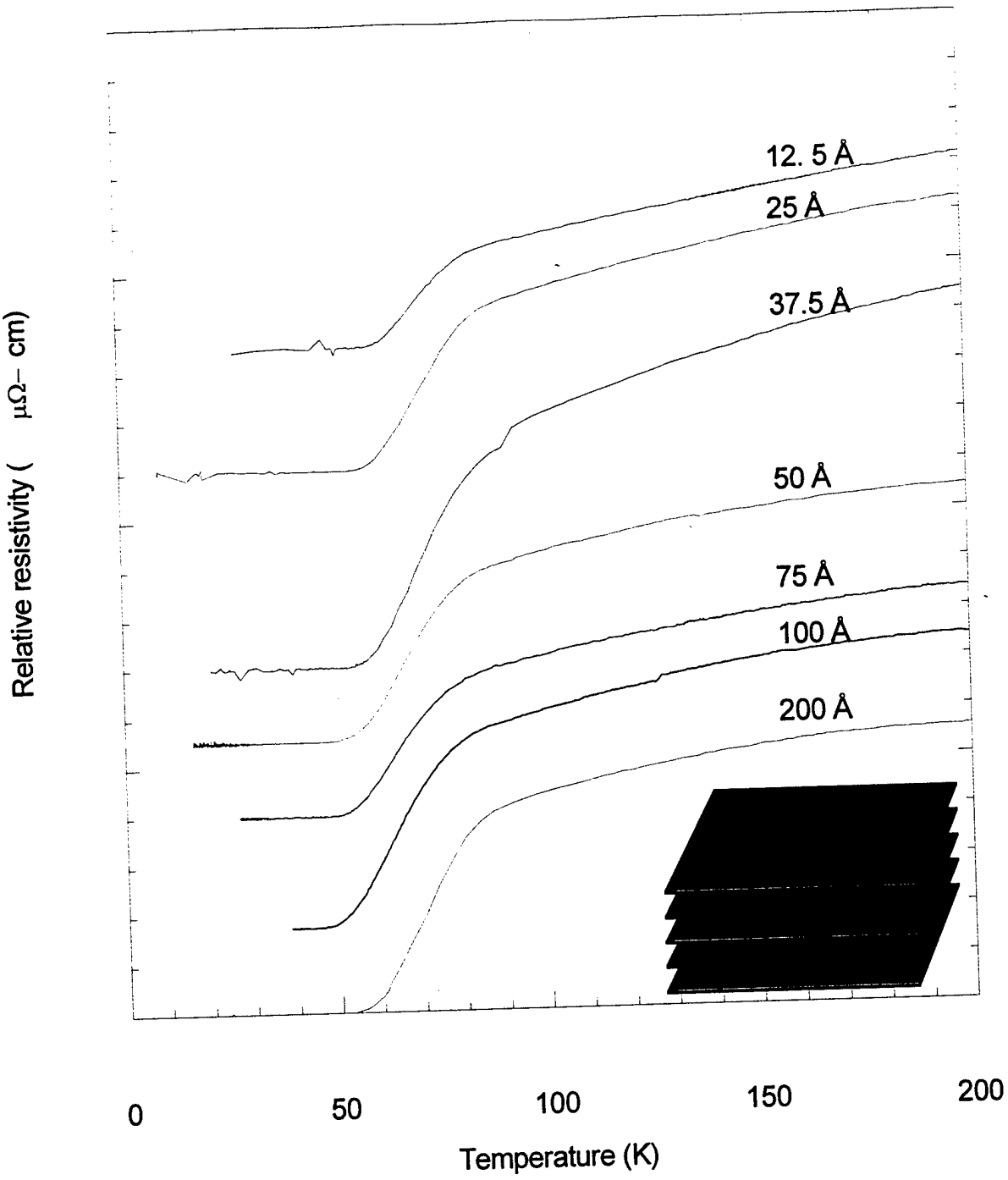

Figure 15 Relative resistivity vs. temperature for 5 layers of A (60 Å)/YBCO (37.5 Å)/ A (varied)/YBCO (37.5 Å)/ A (200 Å) superlattices with PBCAO thickness varied , where A = PBCAO.

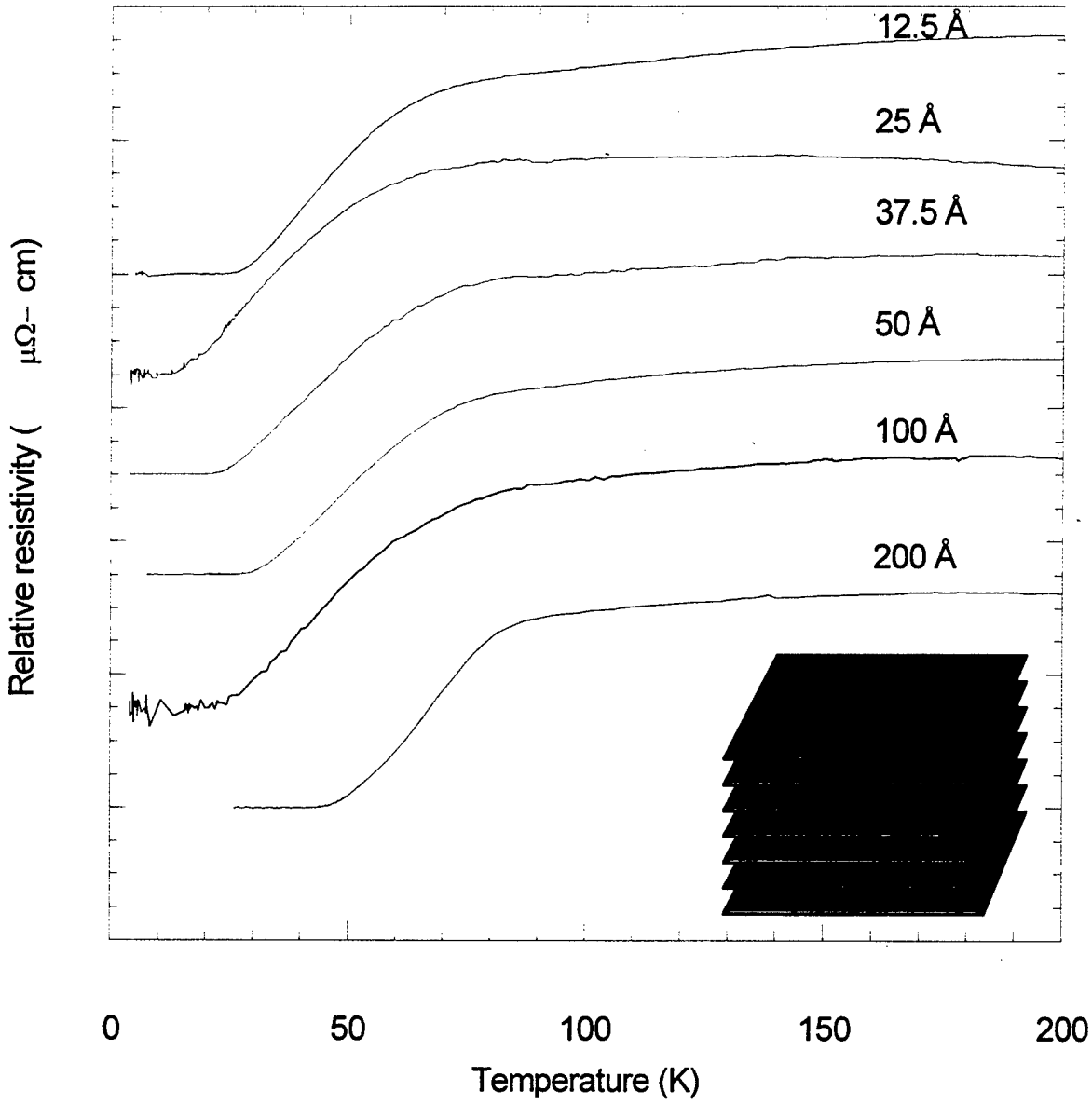

Figure 16. Relative resistivity vs. temperature for 7 layers A (60 Å)/YBCO (37.5 Å)/A/YBCO (37.5 Å)/A/YBCO (37.5 Å)/A (200 Å) superlattices with PBCAO thickness varied, where A = PBCAO.

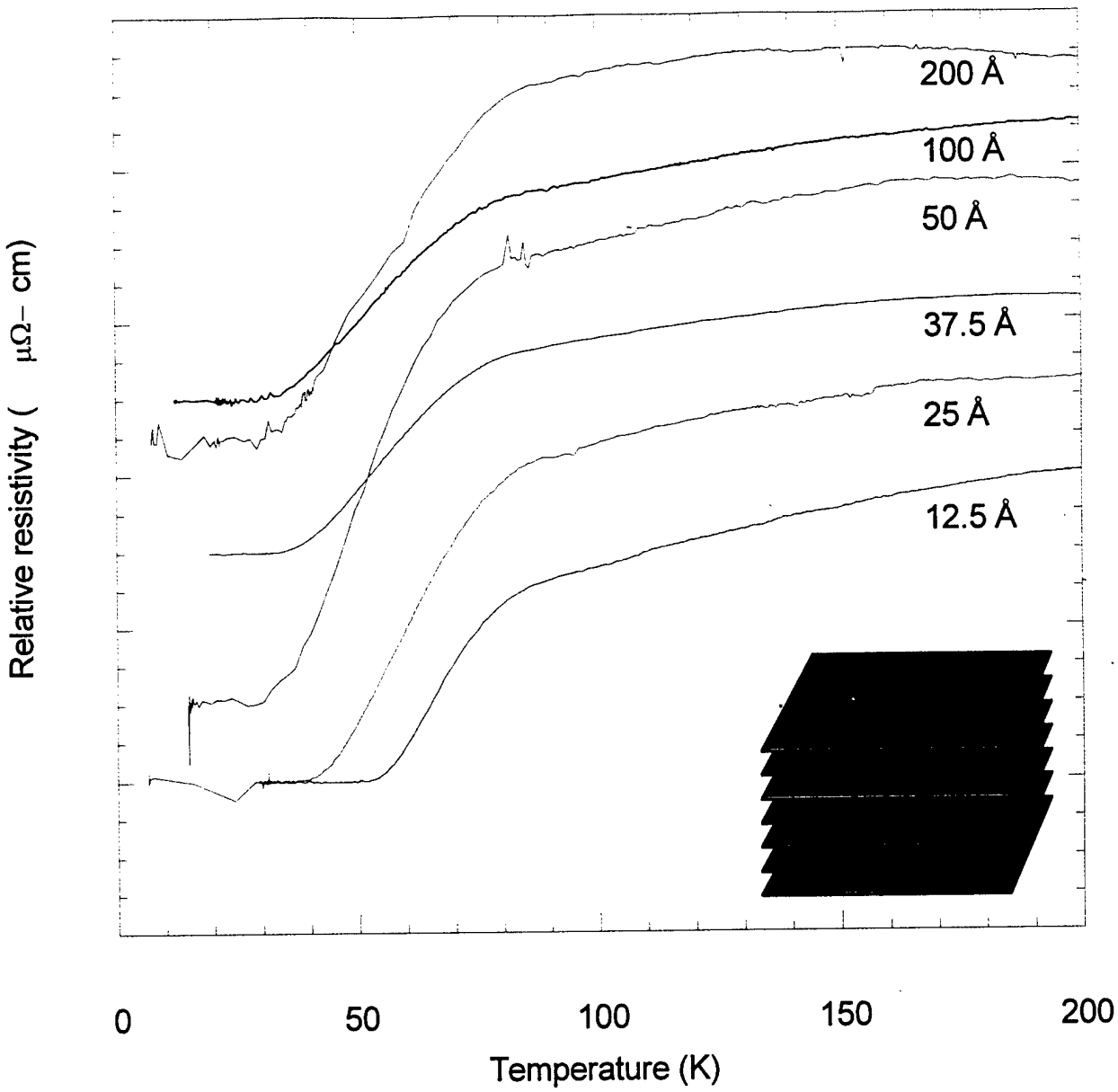

Figure 17. Relative resistivity versus temperature for 7 layers of G (60 Å)/ YBCO (37.5 Å)/ G/YBCO (37.5 Å)/G/YBCO (37.5 Å)/G (200 Å) superlattices with PBCGO thickness varied, where G = PBCGO.

Figure 13 shows the resistivity vs. temperature for multilayers made of (a) PBCAO and (b) PBCGO buffer layers for 37.5 Å YBCO thick films. Within Experimental uncertainty the T_c of the superlattices are the same for a given thickness of YBCO films in spite it is a trilayer, 5, or 7 layer superlattice. Figure 14 and 15 show the relative resistivity versus temperature plots for 5 layers A (60 Å)/YBCO (37.5 Å)/ A (varied)/ YBCO (37.5 Å)/A (200 Å) and G (60 Å)/YBCO (50 Å)/ G (varied)/ YBCO (50 Å)/ G (200 Å) multilayers with the buffer layer thickness A ≡ PBCAO and G ≡ PBCGO varied. Figure 16 and 17 are the corresponding plots for 7 layers of YBCO/PBCMO superlattices. Within experimental uncertainty the onset T_c for all superlattices of same YBCO thickness are the same. If two-dimensional superconducting transition exists in YBCO, its T_c should be lower or at most equals to the lowest T_c of all superlattices which is 50 K for d = 25 Å. The highest T_c of all superlattices in this experiment is 90 K. Therefore coupling between CuO_2 planes at least contributes 40 K to the T_c of YBCO. If the coupling length is about 100 Å and if proximity effect exists in PBCAO and PBCGO like that of PBCO then superlattices made of thinner buffer layers should have higher T_c because coupling between nearest YBCO layers which has shorter distance should increase T_c. The fact that same onset T_cs for all superlattices of same d in Figures 14 – 17 in spite of the thickness of the buffer layer indicates that the buffer layers, even as thin as one unit cell (~12 Å), can effectively cut of the coupling so that no coupling between YBCO layers exists. Figure 13 shows even stronger evidence on the absence of interlayer coupling between nearest YBCO layers. In a trilayer superlattice, there is only one YBCO layer and thus no inter YBCO layer coupling. If the onset T_cs for the 5 and 7 layers superlattices are the same as the trilayer one, then coupling between nearest YBCO is totally cut off and the PBCAO and PBCGO should be excellent I layers.

III. Conlusion

We have synthesized $PrBa_2(Cu_{1-x}M_x)_3O_{7-\delta}$, for M= Al, Co, Fe, Ga, Ni, and Zn, and x = 0.05, 0.10, 0.15, and 0.20 by means of solid state reaction. We utilized x-ray diffraction method to study the structure and the standard four probes technique to study transport property of the bulk PBCO and PBCMO samples. All of the samples in this study have orthorhombic structure and are belong to the space group *Pmmm*. Their lattice parameters are all very close to those of YBCO. All of the samples do not show significant second phase except the 15% or higher Ni and Zn-doped ones. The second phase in these samples are identified mainly to be $BaCO_3$. This indicates that solubility of Ni and Zn is substantially lower than that of Al, Fe, Ga, and Co dopants. This observation may imply that Ni and Zn prefer a different site than Al, Fe, Ga, and Co ions. For YBCO it is commonly accepted that Ni and Zn substitute preferentially in the CuO_2 planes i.e. the Cu(2) sites, while Al, Co, Fe, and Ga in the CuO chains, or Cu(1) sites. It is experimentally verified that the Cu(2) site has a valence of +2 which matches the valence of Zn^{2+} and Ni^{2+} ions well. On the other hand, the Cu(1) site is either in the +3 valence state or in the +2 and +3 mixed-valence states which make it favorable for Al^{3+}, Co^{3+}, Fe^{3+}, and Ga^{3+} ions.

Takenaka *et al.* [K. Takenaka, Y. Imanaka, K. Tamasaku, T. Ito, and Uchida, Phys. Rev. B **46,** 5833 (1992)] performed polarized optical reflectivity study on PBCO and found that hole concentration in the CuO_2 planes is very low and hole dope to the planes are very difficult even under full oxygenation. For this reason, the CuO_2 planes in PBCO are non-conducting. Based on the optical reflectivity data and the assumption that no oxygen holes in the CuO_2 planes,

Fehrenbacher and Rice [Phys. Rev. Lett. **70**, 3471 (1993)] performed calculation on the electrical conduction in PBCO and found that there is 0.5 hole per Cu atom in the CuO chains. The chains in PBCO may conduct locally.

If Ni and Zn can only go to the Cu(2) sites then Ni and Zn doped samples will not increase resistivity, because the planes do not have many holes to be filled and thus resistivity cannot increased by much. This is in agreement with the lowest increased in resistivity observed for the Ni and Zn doped sample in this experiment. On the other hand, if Al, Fe, Ga, and Co may go either to the Cu(1) and the Cu(2) sites as was found in YBCO, then the fact that the solubility of Ni and Zn is lower than that of Al, Fe, Ga, and Co is obvious. Our findings that the substituting level of Ni and Zn for Cu in PBCO is limited to 15% while the solubility of Al, Fe, Ga and Co is higher than 20% are in agreement with those observed for YBCO. Our finding that resistivity increase for Al, Ga, Fe, and Co doped samples are higher than that for No and Zn can be explained by the formers may also occupy the Cu(1) sites. Occupying Cu(1) site may fill the O 2P hole and block electrical conduction. However, Fe, Ni, and Co are magnetic and have magnetic moment which may break Cooper pair. The T_c of the YBCO/PBCMO multilayers may decrease if the doping element migrates from the PBCMO layers into the YBCO layers. Comparing all doping elements, Fe, Ni, Co and Zn will lower T_c more than Al and Ga. Fe, Ni, Co and Zn doped PBCO may not be ideal buffer layer for YBCO/PBCMO multilayers. Al and Ga-doped samples are non magnetic and their electrical resistivities are the highest and the second highest. Therefore, we believe that Al and Ga-doped materials may be well suited to be the buffer layers in YBCO/PBCMO multilayers.

High quality expitaxy 3, 5, 7, and 9 layers of YBCO/PBCAO and YBCO/PBCGO multilayers were grown in this research. Multilayers of 1, 2, 3, 4, 5, 6, 8, and 16 unit cell thick YBCO layer were fabricated. Transport studies were carried out from room temperature down to 4.2 K. No superconducting transition above 4.2 K was observed for multilayers made of 12.5 Å thick YBCO layer. YBCO samples made of more than a unit cell thick is needed for superconductivity to occur. It is not clear that stress from the substrate destroys the superconductivity or two-dimensional superconductivity does not exist in YBCO superconductor.

In this research,, T_c of the multilayers is found to increase when the thickness of YBCO is increased. This indicates coupling between YBCO unit cells help superconductivity. T_c, however, levels off when the thickness of YBCO layers reaches 100 Å. This implies that the coupling length for YBCO is about 100 Å. On the other hand, the T_c's for all superlattices of same YBCO thickness are the same in spite of the superlattice is made of 1, 2, 3, 4, 5, 6, 8, or 16 unit cell thick or 12.5 Å, 25 Å, 37.5 Å 50 Å, 75 Å, 100Å or 200 Å thick of the buffer layer. This result indicates that the PBCMO buffer layers can effectively cut off the coupling between neighboring YBCO layers made on both sides of the buffer layer even when the buffer layer is as thin as 12.5 Å. This is contrary to the findings by other groups in which T_c decreases with increasing the thickness of PBCO buffer layer. Comparing the experimental results of superlattices using PBCMO and PBCO as buffer layers, it is obvious that the PBCO buffer layers used by other groups failed to insulate neighboring YBCO layers so that coupling between adjacent YBCO layers exists either through proximity effect of YBCO on PBCO or through other charge transformation mechanism.

Although no superconducting transition was found for unit cell thick YBCO films in superlattices we cannot rule out the existence of 2-D superconducting transition in YBCo for two reasons: First our setup is limited to 4.2 K. We cannot detect superconducting transition below this temperature. Second even though the lattice match between PBCMO and YBCO is excellent, a small mismatch in lattice parameters does exist. We do not know the effect of the stress due to the mismatch affect superconductivity in YBCO. Better data analysis or other experiment may be needed to give a conclusion on 2-D superconducting transition for YBCO.

We believe that 20% Al and Ga-doped PBCO materials are much superior than the undoped PBCO to be used as the I-layer for SIS Josephson junctions and devices. We have just been funded by the Department of Defense to carry out Josephson junction and devices using PBCAO as the I – layer.